Scripta Materialia 132 (2017) 53–57

Contents lists available at ScienceDirect

Scripta Materialia

journal homepage: www.elsevier.com/locate/scriptamat

Regular Article

A chevron-notched bowtie micro-beam bend test for fracture toughness measurement of brittle materials

Fiona Yuwei Cui *, Richard P. Vinci

Department of Materials Science and Engineering, Center for Advanced Materials and Nanotechnology, Lehigh University, Bethlehem, PA 18015, United States

ARTICLE INFO

Article history:
Received 17 January 2017
Received in revised form 27 January 2017
Accepted 27 January 2017
Available online 3 February 2017

Keywords:
Fracture
Toughness
Bending test
Glass
Zerodur

ABSTRACT

A micro-mechanical fracture testing method has been developed that uses a bowtie-shaped micro-beam specimen with a chevron notch. This clamped-clamped specimen can produce stable crack growth in brittle materials. Cyclic loading causes progressive crack extension, thereby producing multiple fracture toughness results in one experiment. The symmetric geometry eliminates the mixed mode fracture that exists in single-ended cantilevers. A 3D finite element analysis model was used to relate the crack length to the beam compliance, and then to the fracture toughness. The results of tests using fused quartz and glass-ceramic materials match very well with published fracture toughness values.

Traditional mechanical testing methods developed for bulk materials are often difficult or impossible to apply directly to small-scale specimens, due to sample handling challenges and the small loads and displacements involved. While a number of techniques now exist for measuring elastic and plastic properties of thin films and microstructural constituents, measurement of fracture toughness still presents a number of challenges. The micro-cantilever deflection test has recently emerged as a preferred method due to the simplicity of the cantilever beam configuration. It has been utilized to analyze structure-property relationships in a variety of materials such as thin films and individual phases within multiphase materials, and different phenomena including the influence of impurity segregation on grain boundary mechanical behavior [1–4].

While cantilevers have a number of advantages for micro-scale fracture testing, the inherent mixed mode fracture cannot be neglected at large deflections and in anisotropic materials, and the difficulty in producing a truly sharp crack by fatigue or other methods makes the fracture results sensitive to the radius of the pre-machined notch. Moreover, regardless of the specific specimen shape, site-specific micro-scale sample fabrication typically requires techniques that are time consuming and costly. Generating sufficient fracture data to ensure statistical significance is often not practical for any configuration that results in a single data point per test specimen. Recently, stable crack growth has been achieved in cantilevers milled with a chevron notch on the top surface; in this way there is sufficient stability to reliably produce a truly sharp crack prior to the onset of failure [5], but the mixed mode fracture toughness effect due to the asymmetric geometry of a cantilever is still present and each specimen yields only a single fracture toughness value. A symmetric clamped-clamped beam with a straight notch on the underside has been explored as a way of eliminating the mixed mode fracture, and has been shown to achieve stable crack growth under certain conditions [6]. However, the high stresses induced at the clamped ends can cause nearly simultaneous failures at the beam center and ends, complicating analysis and limiting the number of stable fracture events that can be measured [7].

To address these shortcomings, we have developed a bowtie-shaped beam configuration that is fixed at both ends, and that has a chevron notch milled into the underside at the beam center, as shown in Fig. 1. The stiff, symmetric test specimen configuration with a centralized chevron notch allows the controlled propagation of a crack advancing along a straight path. This makes it possible to collect multiple measurements of toughness with a single specimen by cyclically loading to a series of increasing peak load values, each of which causes a small, stable, and measureable increase in crack length. The specimen configuration also eliminates mixed mode fracture toughness. The milling time needed to create such a specimen is only about 25% greater than to create a standard cantilever.

The loading point is located directly above the chevron notch in the middle of the beam. When loading, the tip of the chevron notch will be the highest stress concentration, and thus the preferred site for crack initiation. As the crack advances along the chevron notch, the crack-front length will increase, as shown in Fig. 2a, thus a higher load is required for further propagation in each step [8,9]. Under appropriate testing conditions, such as the right chevron geometry and a very stiff loading instrument, the crack would advance in a stable fashion and

* Corresponding author.
E-mail address: fiona.yw.cui@gmail.com (F.Y. Cui).

http://dx.doi.org/10.1016/j.scriptamat.2017.01.031
1359-6462/

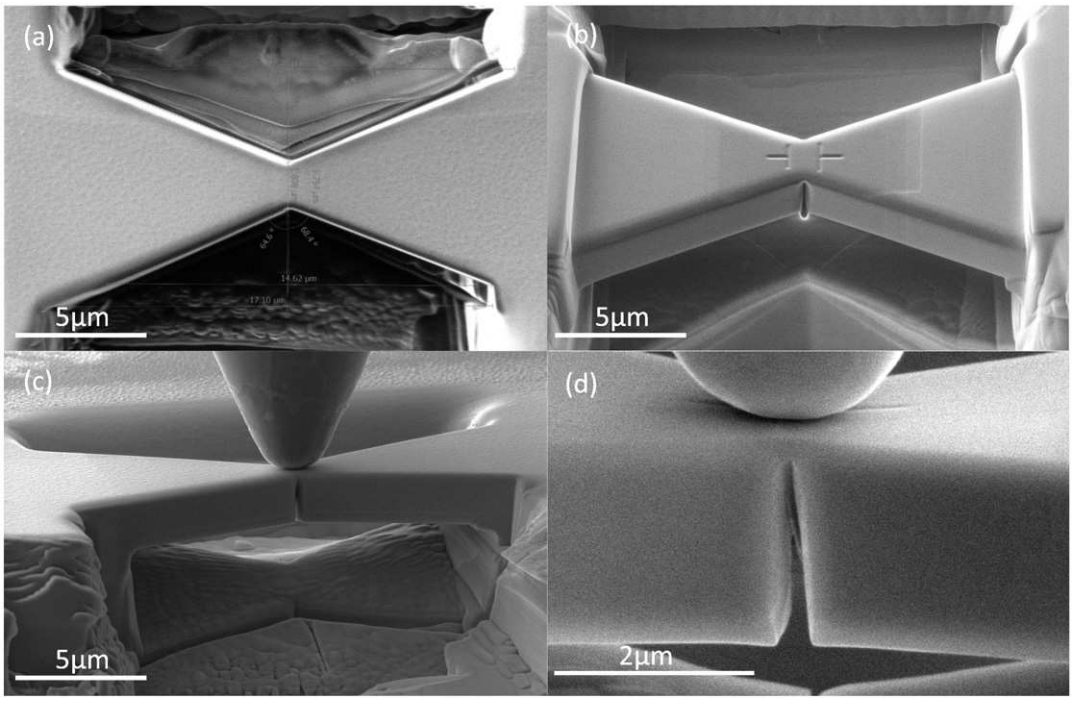

Fig. 1. Fused quartz bowtie chevron-notched specimen fabricated with Focused Ion Beam milling. (a) top surface of a bowtie chevron beam, (b) 30° view of a bowtie specimen, (c) in-situ mechanical test with indenter on top of specimen, (d) crack propagation visible under SEM observation during in-situ test.

the extent of crack propagation could be controlled by the applied maximum load. If a cyclic load-unload function is employed, the compliance change from one cycle to the next is a predictable measure of crack propagation [10]. This correlation enables the measurement of compliance as a function of crack length, the crack advance per load cycle, and the fracture energy associated with the corresponding maximum load value at each step.

A bowtie shaped specimen was selected to avoid the end-cracking often observed in rectangular clamped-clamped specimens. Experience with chevron-notched rectangular beams demonstrated that the ends of the beam would sometimes simultaneously fracture in a catastrophic fashion so that the real crack propagation at the chevron notch was hard to distinguish [7]. A triangle-shaped specimen has a reduced stress concentration at the beam ends as compared to a specimen with a uniform cross-section [11]. This eliminates or delays the end-cracking, allowing the central crack to initiate and propagate at the notch area for evaluation of the fracture toughness value.

In the examples reported here, each specimen was fabricated from a bulk fused quartz or lithium-aluminosilicate glass-ceramic (Zerodur™) sample. These two materials were selected because they both are amorphous brittle materials, so the fracture toughness measurements will not be affected by anisotropy or plasticity. Furthermore, published fracture toughness values for both materials are available for comparison.

The test specimens were made using Focused Ion Beam (FIB) milling in an FEI Scios instrument. The bulk sample was first mechanically ground and polished on two adjacent surfaces so that a 90-degree edge was exposed for FIB milling. After the basic shape was established using a high ion beam current, the test structure was ion polished using 0.1 nA at a tilt angle of $\pm 1.5°$ to ensure smooth surfaces with minimal ion damage and parallel sides. The chevron notch was fabricated by milling at an angle to the surface in three steps, starting with an ion beam current of 10 pA with a larger width milling pattern, reducing to a smaller width, and finishing with 1.5 pA and a minimum milling width. Thus, a 'V' shaped segment was generated in the center of the

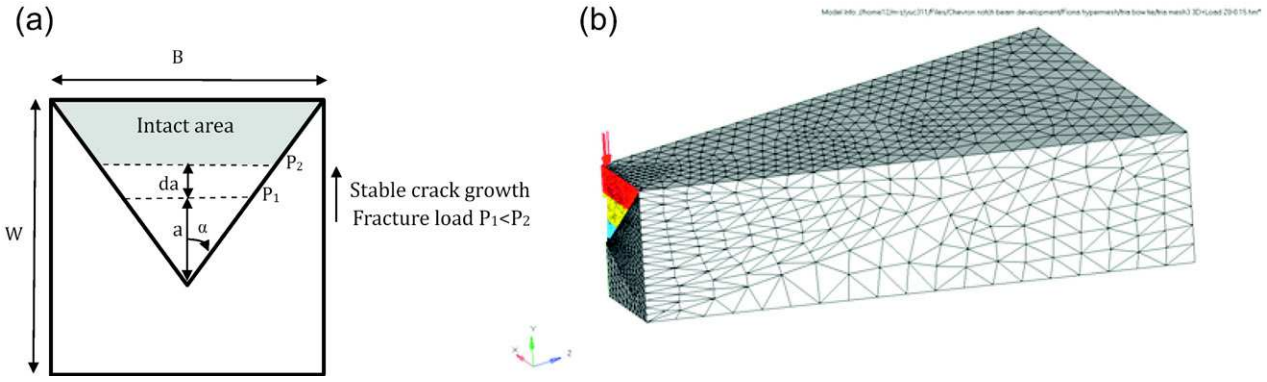

Fig. 2. (a) Schematic cross-section of the bowtie chevron-notched beam design, showing the chevron notch during crack propagation. The triangle represents the original intact region and the grey area represents the intact region after some degree of crack growth has occurred. (b) Quarter symmetry FEA model. Axial displacement constraints (z-axis) were applied at the intact area ahead of the crack front, where different color highlights represent different crack lengths.

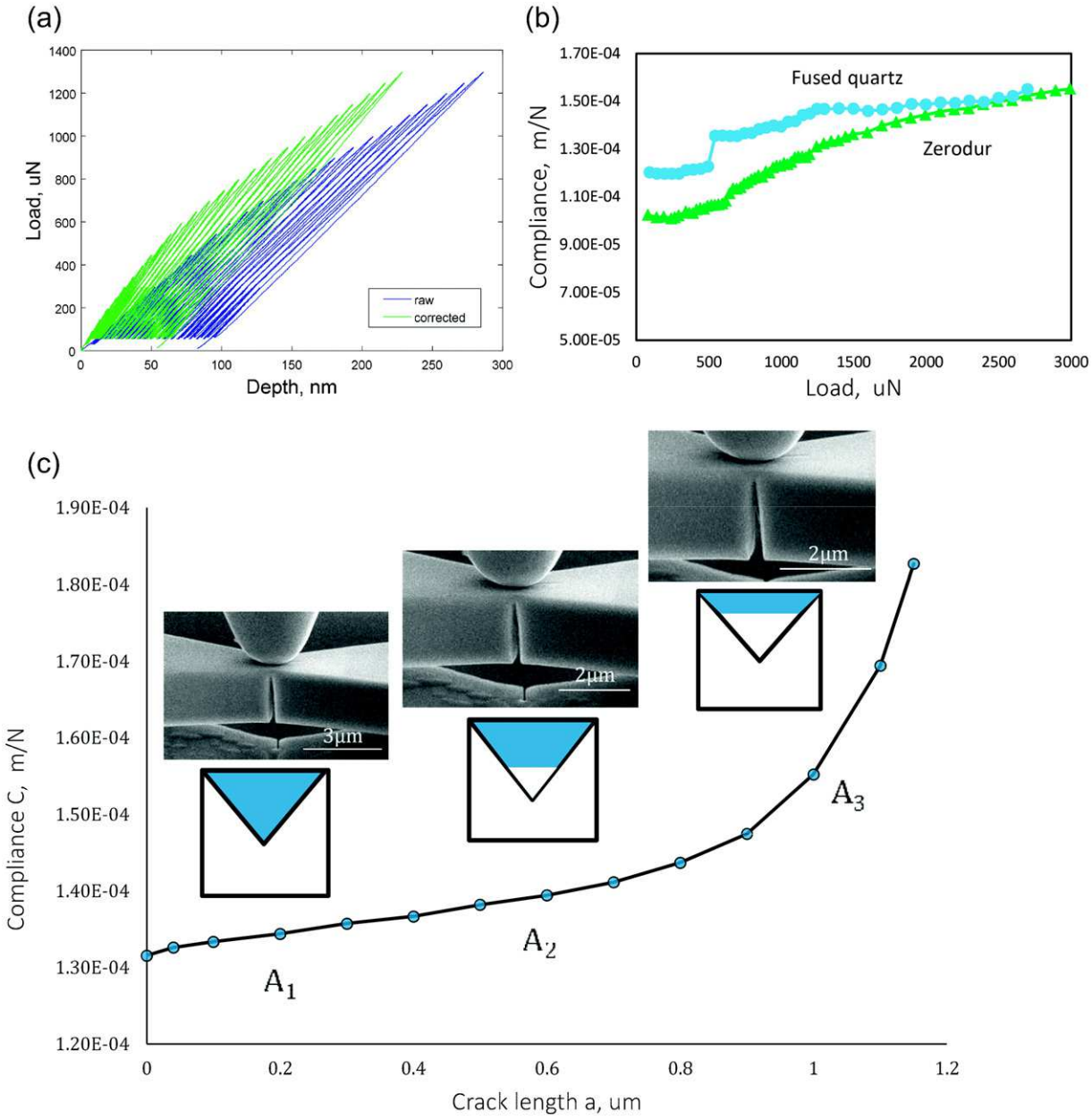

Fig. 3. (a) Contact stiffness correction of Load-displacement curve of Fused Quartz specimen (b) Compliance change in each unloading segment with respect to load for fused quartz and zerodur (c) Finite element analysis result of compliance change with respect to crack propagation length *a*.

test beam with the smallest radius at the tip of the resulting chevron notch, to ensure a reasonably sharp pre-notch for crack initiation. Finally, alignment markers were milled into the top surface to guide placement of the loading tip.

In order to achieve the stability of crack growth, the geometry of the specimen (height, length, width of the beam, notch area thickness, and notch ratio), misalignment tolerance, testing rate, and instrument stiffness all play important roles [8,9]. The specimen dimensions were selected with these criteria in mind. For the current study, the bowtie specimen in Fig. 1 had a nominal length L of 14 μm, a width B of 8 μm at the end of the beam and 2 μm at the middle of the beam, and a thickness W of 2 μm, which produces a square cross section of the notch area

Table 1
Fused quartz fracture toughness value comparison with literature.

Testing method	Fracture toughness value MPa$\sqrt{m}$	References
Macroscopic three-point bending	0.58	Harding et al. [13]
Macroscopic chevron-notched short rod	0.735	Barker [14]
Nanoindentation toughness, cube corner tip	0.6 ± 0.1	Scholz et al. [15]
Microcantilever beam chevron	0.65 ± 0.04	Mueller et al. [5]
Microcantilever chevron triangular	0.67 ± 0.01	Žagar et al. [16]
Microscopic bowtie chevron	0.62 ± 0.07	this study

Table 2
Zerodur™ fracture toughness value comparison with literature.

Testing method	Fracture toughness value MPa$\sqrt{m}$	References
Microindentation toughness, Vickers	0.9	Viens [18]
Microindentation toughness, Vickers	1.33 ± 0.08	Bouvier et al. [17]
Microscopic bowtie chevron	1.26 ± 0.1	This study

of 2 μm × 2 μm. The radius of the sharp notch tip was measured to be 10–20 nm using a Scanning Electron Microscope (SEM), and the widest area of the notch closer to the side surface is 30–50 nm.

A 3D finite element analysis (FEA) quarter-model was built using Altair Hypermesh and ANSYS Mechanical APDL to evaluate the effects of geometry, and to establish the correlation between specimen compliance and crack propagation. A refined mesh at the notch area was used to ensure accuracy of the FEA model, as shown in Fig. 2b. The model dimensions matched the experiment design. The wide end was constrained in all directions to simulate the attachment to the bulk material, the straight side area in the middle of the beam was constrained in the x (transverse) direction to impose model symmetry, and the intact V-notch area was constrained in the z (axial) direction. A distributed load was added on the top surface of the elements above the notch area. A series of models with different crack opening length a were modeled under the same boundary conditions and load conditions to simulate the crack propagation. The intact area for one such case is depicted in Fig. 2a, and a series of areas are shown by the colored regions in Fig. 2b. By analyzing the deflection at the tip of the notched region for each applied load value, a function describing the beam compliance C as a function of crack length a was obtained for each material, as shown in Fig. 3c. Actual specimen dimensions measured in the SEM were used for all calculations rather than the nominal dimensions described above. A sensitivity analysis indicated that uncertainties in the beam length and thickness dimensions strongly influence the results while the chevron dimensions are much less critical.

A nanomechanical testing system (Hysitron PI-85) was utilized to carry out the in-situ fracture toughness testing inside the FEI Scios FIB/SEM. The load and tip displacement (a measure of beam deflection) were recorded simultaneously throughout each test. A visual record was also captured during each test. Tip alignment was facilitated by the SEM environment. As shown in Fig. 1c, the indenter tip is aligned to the middle of the top surface of the specimen. Operating under load control, the specimen was deflected as the load increased, inducing crack initiation at the tip of the chevron notch. A cyclic load sequence with a loading rate of 150 μN/s was utilized. In each load cycle, the specimen was loaded to a certain maximum value to propagate the crack, unloaded, reloaded to a fixed value of 200 μN, and unloaded again to evaluate the beam compliance from the unloading slope. During the next cycle the maximum load value was increased by 25 μN, but the compliance evaluation load of 200 μN was kept the same. The load-displacement results of one test are shown in Fig. 3a. A video of an in-situ mechanical test of Zerodur™ specimen is shown in Video 1.

Prior to analyzing the beam compliance and fracture toughness, it was necessary to correct for the contact stiffness between the indenter tip and the specimen surface. Due to the creation of an indenter impression on the top surface of the specimen, both elastic and plastic deformation needed to be taken into account when analyzing the experiment results. In every loading segment that exceeds the maximum load of any previous cycle, both elastic deformation and new plastic deformation based on the instantaneous load must be known in order to correctly determine the beam displacement from the tip displacement [12]. During unloading and during any reloading region that is lower than the prior maximum load, only the elastic deformation and prior plastic deformation need to be subtracted. An example of a corrected data set is shown in Fig. 3a. Thermal drift of the indenter tip was also calibrated with a separate set of tests, where a typical drift rate of 2 nm/s was obtained. The indentation and fracture tests were limited to around 3–4 min each to minimize the thermal drift effect.

Once the contact stiffness and thermal drift corrections were applied, a decrease in the slope of one compliance evaluation unload segment to the next indicated a compliance change due to stable crack growth. The compliance data was extracted from each unloading slope and plotted with respect to the maximum applied load in Fig. 3b. Fracture toughness then was evaluated using an energy balance approach based on the measured compliance change and corresponding load data, combining the results from the experiment and FEA model. The strain energy release rate G was obtained as a function of compliance change as the crack propagates, which is derived for the chevron notch in our configuration as shown in Eq. (1),

$$G = \frac{1}{2b} P^2 \frac{dC}{da} \tag{1}$$

where P is the maximum load in each loading cycle, b is the notch width at the crack front, defined as $b = 2 \times a \times \tan\alpha$, a is the crack propagation length, and α is the semi-angle of the chevron notch, as shown in Fig. 2a. The quantity $\frac{dC}{da}$ is the compliance change as the crack propagates during each loading cycle. The crack propagation length a and rate $\frac{dC}{da}$ are obtained by combining experiment output, FEA modeling, and numerical methods using MATLAB. If the material is brittle and isotropic, the stress intensity factor at fracture, K_I, can also be obtained by the relation,

$$K_I = \sqrt{\frac{EG}{1-\nu^2}} \tag{2}$$

where E is the elastic modulus and ν is the Poisson's ratio. A fracture toughness value could then be calculated based on Eq. (1) for each unloading segment, and multiple results from a single specimen could be averaged to create a final value and a statistical distribution.

Comparisons between the fracture toughness values measured in this study and literature results are shown in Tables 1 and 2. The fused quartz results represent 27 data points extracted from 3 bowtie specimens. An average fracture toughness value of 0.62 ± 0.07 MPa$\sqrt{m}$ was obtained for the fused quartz, which matches very well with those results that have been reported in the literature [5,13–16]. There are many published measurements of fused quartz fracture toughness so the reported values are likely to be reliable. Unfortunately, there are very few fracture toughness measurements reported for Zerodur ™. The glass-ceramic results from the bowtie structure represent 28 data points extracted from 4 specimens. The average value of 1.26 ± 0.1 MPa$\sqrt{m}$ for the glass-ceramic matches well with a 2004 report that used microindentation [17]. An older report that also used microindentation claimed a value between that of fused quartz and the newer Zerodur™ result [18]. While the match between the older value and the current measurement is not very close, both values agree insofar as the glass-ceramic has a higher fracture toughness than fused quartz. In aggregate, the current results strongly support the chevron-notch bowtie as a promising test structure for micro-scale fracture toughness testing of brittle materials.

Supplementary data to this article can be found online at http://dx.doi.org/10.1016/j.scriptamat.2017.01.031.

Acknowledgment

This material is based upon work supported by the National Science Foundation under Grant No. CMMI-1436585.

References

[1] K. Takashima, S. Koyama, K. Nakai, Y. Higo, Mat. Res. Soc. Symp. Proc. 741 (2003) 1–6.
[2] K. Matoy, H. Schönherr, T. Detzel, G. Dehm, Thin Solid Films 518 (2010) 5796–5801.
[3] W. Cao, A. Kundu, Z. Yu, M.P. Harmer, R.P. Vinci, Scr. Mater. 69 (2013) 81–84.
[4] D.E.J. Armstrong, A.J. Wilkinson, S.G. Roberts, Philos. Mag. Lett. 91 (2011) 394–400.
[5] M.G. Mueller, V. Pejchal, G. Žagar, A. Singh, M. Cantoni, A. Mortensen, Acta Mater. 86 (2015) 385–395.
[6] B.N. Jaya, S. Bhowmick, S.A.S. Asif, O.L. Warren, V. Jayaram, Philos. Mag. 95 (2015) 1945–1966.
[7] B.N. Jaya, V. Jayaram, Int. J. Fract. 188 (2014) 213–228.
[8] G.T.H.G. Tattersall, J. Mater. Sci. 1 (1966) 296–301.
[9] ASTM Standard C1421-15, ASTM International, West Conshohocken, PA, 2014 1–133.
[10] R.J. Sanford, Principles of Fracture Mechanics(NJ) 2003 247–248.
[11] J.N. Florando, W.D. Nix, J. Mech. Phys. Solids 53 (2005) 619–638.
[12] D. Kupka, E.T. Lilleodden, Exp. Mech. 52 (2012) 649–658.
[13] D.S. Harding, W.C. Oliver, G.M. Pharr, MRS Proc. 356 (1994) 663–668.
[14] L. Barker, Fracture Mechanics Applied to Brittle Materials, ASTM STP 678, ASTM International, 1979 73–82.
[15] T. Scholz, G.A. Schneider, J. Muñoz-Saldaña, M.V. Swain, Appl. Phys. Lett. 84 (2004) 3055–3057.
[16] G. Žagar, V. Pejchal, M.G. Mueller, L. Michelet, A. Mortensen, Scr. Mater. 112 (2016) 132–135.
[17] C. Bouvier, J.C. Lambropoulos, S.D. Jacobs, Opt. Soc. Am. 2 (2004) 4–6.
[18] M.J. Viens, NASA Tech. Memo 4185 (1990).